



EVALUATING THE PERFORMANCE OF GPS-BASED NAVIGATION SYSTEMS DURING GEOMAGNETIC STORMS USING DIFFERENT PSEUDORANGE MEASUREMENTS

¹Adewale, A.O., ¹Oyeyemi, E.O., ¹Oyebola, O.O., ¹Odeyemi, O.O., ¹Olugbon, B., ^{*}¹Odetola, J.A., ¹Akindolire R.T., ²Obafaye, A.A.

¹Department of Physics, University of Lagos, Lagos, Nigeria

²Space Environmental Research Laboratory, National Space Research and Development Agency, Abuja, Nigeria

*Corresponding authors email: aadewale@unilag.edu.ng

ABSTRACT

Geomagnetic storms have significant space-weather effects on space and ground-based Global Positioning System (GPS). The signals from GPS suffer degradation and delay during propagation from space to ground-based receivers, as they travel through the ionosphere. Comparison of GPS positioning 3-D vertical (MRSE) and horizontal (DRMS) root mean squared positioning errors obtained from different pseudorange measurements at low, mid and high latitude stations has been reported. GPS observation data were examined from 6th-12th November 2004, using different pseudorange measurements. Our results show that geomagnetic storms and latitudinal variation have little significance on the positioning. Dual frequency receivers recorded low errors compared to single frequency receivers. Generally, single-frequency GPS receivers on L1 C/A and L1 P codes measurement are more accurate and reliable than the one on L2 P-code. Measurement on the ionosphere-free combination dual frequency receivers (C/A on L1 and P on L2) recorded more significant errors compared to the ionosphere-free L1/L2 combination (P on L1 and P on L2). Our results show that other factors played a significant role in poor positioning errors.

Keywords: geomagnetic storms, pseudorange measurements, TEC, propagation delay, Global Positioning System

INTRODUCTION

Global Navigational Satellite System (GNSS), like the Global Positioning System (GPS), transmit radio signals through the ionosphere which are received by ground-based receivers. Ionospheric irregularities can cause substantial degradation in the performance of GPS for navigational purposes. The radio signals from space-based transmitters undergo propagation delay, which mainly depends on the ionospheric total electron content (TEC), as they traverse the ionosphere. One of the significant sources of signal degradation is the atmospheric (ionospheric and tropospheric) propagation delays, which affects the quality of GPS positioning results. The delay is directly proportional to the number of electrons and inversely proportional to the square of propagation frequency (Park and Gao, 2008 and Trajkovski *et al.*, 2010), leading to an error in the range measurements and these have significant effects on navigation (Kintner and Ledvina, 2005). The usefulness of GPS exists in its accuracy for surveying, geodesy, navigation, and geophysics. GPS signals are delayed relative to the speed of light in a vacuum as they propagate through the ionised region of the ionosphere due to the presence of free electrons (Adewale *et al.*, 2012). This is the primary cause of the range errors, which will consequently lead to positioning errors. These positioning errors vary from one region to the other depending on the solar activity and the geodetic coordinate of the region. A pseudorange is the approximate distance from the transmitting GPS satellite to the receiver since the signal is not received immediately after transmission. It is the product of the time taken for the signal reception and the speed of light in air.

Bhattacharya *et al.* (2009) studied the diurnal and seasonal variations of ionospheric time delay during the minimum solar period from January to December 2005. The study reveals that the equinox season shows the maximum delay while summer gives the moderate and winter shows the minimum time delay. Bhattacharya *et al.*, (2008) investigated the effect of magnetic activity on ionospheric time delay at low latitude station, Bhopal (geom. lat. 23.2°N, geom. long. 77.6°E), using dual frequency GPS measurements. Their results showed that maximum delay was observed during quiet days in equinox months while the delays of the disturbed period are observed during the months of winter. In the work of Adewale *et al.* (2013), it was recorded that during low solar activity, the time delay values are high in equinox months, least during summer and moderate in winter. The correlation between average daytime peak ionospheric time delay and the solar F10.7 flux shows a low positive correlation, with Correlation Coefficient $R = 0.31$ for 2008 and $R = 0.15$ for 2009. Liu *et al.* (2010) showed that the time delays between geomagnetic disturbances and TEC responses depend on season, magnetic local time and magnetic latitude. In the summer hemisphere, at mid- and high latitudes, the negative storm effects can propagate to the low latitudes at post-midnight to the morning sector with a time delay of 4–7 h.

The primary error source in position estimate of GPS is the time delays suffered by radio waves as they propagate through the ionosphere. This is because the ionosphere causes the signal group velocity to slow down and phase velocity to speed up (Kintner and Ledvina, 2005). For navigation and geodesy applications, it is essential to have a reasonable estimation of an

ionospheric time delay to achieve better accuracy in GPS position fixing for navigation.

The ionospheric time delay, $\hat{\partial}t$, can be derived from Maxwell's equations in plasma. Using two of Maxwell's equations:

$$\nabla \times \vec{B} = \mu \left(\vec{J} + \frac{\partial \vec{D}}{\partial t} \right) \quad (1)$$

$$\nabla \times \vec{E} = - \frac{\partial \vec{B}}{\partial t} \quad (2)$$

A Fourier decomposition of equations (1) and (2) with the current density $\vec{J} = n_e q \vec{v}_e$, where n_e is the electron density, q is the charge on an electron, and \vec{v}_e is the instantaneous electron velocity in response to the electric field, yields the result that the group velocity, v_g , is (Bhattacharya *et al.*, 2009)

$$v_g = c \left(1 - \frac{\omega_p^2}{\omega^2} \right)^{1/2} \quad (3)$$

and the phase velocity is

$$v_p = c \left(1 - \frac{\omega_p^2}{\omega^2} \right)^{-1/2} \quad (4)$$

where ω_p is plasma frequency and $\omega_p^2 = \frac{n_e q^2}{\epsilon m_e}$, and m_e is the mass of an electron.

Expanding (3), we have

$$v_g = c \left(1 - \frac{\omega_p^2}{2\omega^2} + \frac{\omega_p^4}{8\omega^4} + \dots \right) \quad (5)$$

The term $\frac{\omega_p^4}{8\omega^4} \ll 1$ at GPS L1 signal frequency ($f_l = 1575.42$ MHz), hence

$$v_g = c \left(1 - \frac{n_e q^2}{2\epsilon m_e \omega^2} \right) = c \left(1 - \frac{40.3 n_e}{f^2} \right) \quad (6a)$$

The group ionospheric time delay, $\hat{\partial}t$, along a path l , can be derived by subtracting the true velocity, v_g , from the assumed velocity, c , and multiplied by the ratio of the travel time of the signal to assumed velocity, and can be expressed as follows:

$$\hat{\partial}t = \frac{1}{c} \int_{path} (c - v_g) dt = \frac{1}{c} \int_{path} \left(\frac{c}{v_g} - \frac{v_g}{v_g} \right) dl \quad (6b)$$

Substituting (6a) into (6b) we have:

$$\hat{\partial}t = \frac{1}{c} \int_{path} \left(\left(1 - \frac{40.3 n_e}{f^2} \right)^{-1} - 1 \right) dl = \frac{1}{c} \int_{path} \left(1 + \frac{40.3 n_e}{f^2} - 1 \right) dl$$

$$\partial t = \frac{40.3}{cf^2} \int_{path} n_e dl = \frac{40.3}{cf^2} TEC \quad (7)$$

where $\int_{path} n_e dl$ is the TEC and f is the carrier frequency.

Conventionally, ionospheric time delay error on GPS signals can be reduced by using the dual-frequency receivers (Kintner and Ledvina, 2005). Dual-frequency GPS receivers operate by comparing the time delay between the two GPS frequencies, $f_1 = 1.57442$ GHz and $f_2 = 1.2276$ GHz and then estimate the TEC. Even though ∂t cannot be measured at a single frequency with a standard receiver clock, the difference in ∂t at two different frequencies can be measured (Bhattacharya et al., 2009). The difference in arrival time for two codes transmitted at identical times but different frequencies can be given as (Bhattacharya et al., 2009):

$$\Delta(\partial t) = \frac{40.3 \times TEC}{c} \left(\frac{f_1^2 - f_2^2}{f_1^2 f_2^2} \right) \quad (8)$$

Especially for single frequency receivers, a suitable ionospheric model is required for GNSS to minimise the ionospheric delay. The early studies mostly focused on the use of different ionospheric empirical models, such as the Bent model (Bent et al., 1976), the Klobuchar model (Klobuchar, 1987), Inverse Distance Weighted (IDW) with Klobuchar model (Prasad and Sarma, 2004), International Reference Ionosphere (IRI) model (Bilitza and Reinisch, 2008) and NeQuick model (Nava et al., 2008). Single frequency L1 C/A receivers employ an ionospheric model (Klobuchar, 1987) that uses eight parameters in the navigation message to estimate ranging errors. Kintner and Ledvina (2005) showed the inadequacies of this model to correctly predict the ranging errors, especially during periods of severe scintillation and geomagnetic storms. The European component of GNSS, GALILEO, uses the NeQuick model (Radicella and Leitinger, 2001; Nava et al., 2008) to correct the ionospheric error contribution to improve the positioning accuracy from single-frequency receivers. Apart from the method of employing ionospheric models to estimate ranging errors for improved navigation accuracy, another technique is to transmit the signals on two frequencies sufficiently far apart that the dispersive effects of propagation through a plasma permit the TEC to be estimated from the differential delay (Kintner and Ledvina, 2005; El-naggar, 2011).

Some researchers have studied the effect of geomagnetic storms and the ionosphere on positioning error and ionospheric time delay; and have reported significant problem for space-based navigation and communication systems (Aaron and Basu, 1994; Groves et al., 2000; Doherty et al., 2000; Bhattacharya et al., 2008; Liu et al., 2010). A geomagnetic storm is caused by solar disturbances such as coronal mass ejections (C.M.E's) and solar flares. The interaction between the flux of charged particles and the earth's magnetic field can cause operational and physical damage to GPS orbiting satellites and equally disrupt electrical grids on the earth surface (Skoneet al., 2001). Vlasov et al. (2003) stated that two factors induce ionospheric disturbances during a geomagnetic storm. They are thermospheric heating, which modifies the wind pattern, and penetration of strong electric fields to low latitudes. It has been extensively reported that the penetrating electric fields can cause a substantial dayside enhancement in TEC (Jakowski et al., 1999; Tsurutani et al., 2004; Sahai et al., 20011; Zhao et al., 2005; Bagiya et al., 2009; Dashora et al., 2009), and the simultaneous response on the nightside shows a decrease in TEC (Jain et al., 2010). During

geomagnetic storms and extreme scintillation events, it has been observed (Jain et al., 2010; Dubey et al., 2006) that ionospheric disturbances cause data loss in satellite communication links and rapid variations of signals from GPS satellite. Skoneet al. (2001) reported that the rapid phase variations might cause a Doppler shift in the GPS signal which may exceed the bandwidth of the phase lock loop, resulting in a loss of phase lock and amplitude fades, and these can cause signal-to-noise-ratio to drop below receiver threshold. These can reduce the availability of satellites for GPS navigation and satellite communication, which may affect GPS positional accuracy, navigational accuracy and the GPS tracking performance at the equatorial region of Africa (Akala et al., 2012, Goswani et al., 2018).

The dual frequency GPS receiver can provide both carrier phase and pseudorange measurements for the two GPS frequencies in the L-band (referred to as Link 1 (L1) and Link 2 (L2)), and the measurements can be used to estimate the position, velocity and time (PVT) in real time. The signal on L1 is transmitted at frequency $f_{L1} = 1575.42$ MHz, and the frequency of L2 is $f_{L2} = 1227.60$ MHz. Apart from the carrier frequencies, each GPS signal consists of a ranging code. The ranging codes consist of a family of binary codes called pseudo-random noise (PRN) sequences or PRN codes which are associated with the two kinds of services rendered by GPS, namely: Standard Positioning Service (SPS) for peaceful civil use and Precise Positioning Service (PPS) for the United States military users (Kintner and Ledvina, 2005, Misra and Enge, 2006). The SPS codes are called coarse/acquisition codes (C/A-codes), and PPS codes are referred to as precision (encrypted) codes or P(Y)-codes. Each GPS satellite transmits a unique C/A-code on L1 and unique P(Y)-codes on both L1 and L2 (Misra and Enge, 2006). The different pseudorange measurements that exist for the estimation of PVT are L1 C/A code, L1P code, L2P code, Ionospheric free L1/L2 combination (C/A on L1 and P on L2) and Ionosphere-free L1/L2 combination (P on L1 and P on L2). Little attention has been paid to GPS estimation of position using different pseudorange measurements. This paper describes the performance of the GPS during geomagnetic storms by comparing the various positioning errors from different pseudorange measurements using data recorded by ground-based receivers at low and high latitude stations. Also, the various ways of mitigating the positioning errors are equally discussed.

DATA AND METHOD OF ANALYSIS

The data used for this research were obtained from the Scripps Orbit and Permanent Array Centre (SOPAC) (<http://sopac.ucsd.edu>). The geographic and geomagnetic latitudes and longitudes of the stations used are shown in Table 1. The disturbed storm times (Dst) indices were obtained from

<http://wdc.kugi.kyoto-u.ac.jp/dstdir/index.html>. GPS observation data were analysed from 6th-12th November 2004, using different pseudorange measurements, i.e., L1 C/A, L1 P, L2 P codes and ionosphere-free combination ((C/A on L1 and P on L2) and (P on L1 and P on L2)). The Geomagnetic latitudes (φ) are used in Equations 9,10 and 11 to define low, mid and high latitude of all stations under consideration.

- Low Latitude Stations $0 \leq \varphi \leq 20$ (9)
- Mid Latitude Stations $21 \leq \varphi \leq 59$ (10)
- High Latitude Stations $\varphi \geq 60$ (11)

The GPS RINEX (Receiver Independent EXchange) format observed pseudorange from several stations were used for reconstruction of the horizontal and vertical GPS positioning performance. The standard (Klobuchar) GPS ionospheric delay correction model and a 30-s sampling were applied. The horizontal positioning error components concerning true positions (along X, Y and Z axis) are computed as follows (Misra and Enge, 2006):

$$\varphi_{E(M)} = \frac{(\varphi_M - \varphi_T) \cdot \pi \cdot R}{180} \tag{12}$$

and

$$\lambda_{E(M)} = \frac{\lambda_M - \lambda_T \cdot \pi \cdot R \cdot \cos\left(\frac{\varphi_M - \varphi_T}{180}\right)}{180} \tag{13}$$

where φ_E = northing error, φ_M = measured latitude, φ_T = true latitude, λ_E = easting error, λ_M = measured longitude, λ_T = true longitude, R = radius of the Earth = 6378137 m.

Different pseudorange measurements, including L1 C/A code, L1P code, L2P code, Ionospheric free L1/L2 combination (C/A on L1 and P on L2) and Ionosphere-free L1/L2 combination (P on L1 and P on L2) were used. The ionosphere-free linear combination of L1 and L2 observations is commonly used in precise global positioning system positioning applications to remove the effects of ionospheric refraction from the data processing (Hofmann-Wellenhof et al. 2001). Each GPS satellite transmits signals on the two L-band frequencies, L1 and L2. The L1 carrier frequency is 1575.42 MHz and has a wavelength of about 19 centimetres. The L2 carrier frequency, however, is 1,227.60 MHz and has a wavelength of about 24 centimetres.

The L1 signal is modulated with a coarse-acquisition code (C/A-code) and a P-code. The L2 signal is modulated with a P-code only. Each satellite carries precise atomic clocks to generate the timing information needed for precise positioning. The absolute value of range accuracies obtainable from the GPS is largely dependent on which code (C/A or P) is used to determine positions. The MATLAB scripts used for this study were written by Dr. John F. Raquet, Air Force Institute of Technology. A 50% relative humidity was used, and a tropospheric (modified Hopfield model) correction was applied. The 2-D and 3-D root mean square error was calculated using

$$2 - D \text{ rms error (DRMS)} = \sqrt{\frac{1}{n} \sum_{j=1}^n (\Delta x_j^2 + \Delta y_j^2)} \tag{14}$$

$$3 - D \text{ rms error (RMSE)} = \sqrt{\frac{1}{n} \sum_{j=1}^n (\Delta x_j^2 + \Delta y_j^2 + \Delta z_j^2)} \tag{15}$$

where Δx_j , Δy_j , and Δz_j are the errors in the east, north and up components of the j th position estimate sample.

The different positioning errors and the plots for easting, northing and up error for the different pseudorange measurements were obtained and analysed.

The dilution of precisions (geometry-dilution of precision (GDOP), position dilution of precision (PDOP), and time dilution of precision (TDOP)) provide a simple characterisation of the user-satellite geometry that affects positioning. The more

favourable the geometry, the lower the dilution of precision (DOP), and the better the quality of the position estimate (Misra and Enge, 2006). We also plot the various DOP against the local time (LT) in other to determine the impact of user-satellite geometry on position accuracy across several stations.

RESULTS

Figure 1 shows the Dst indices for November 2004. Yermolaev *et al.* (2008) reviewed data on observations of the Sun, interplanetary medium, and magnetosphere before and during one of the strongest magnetic storms of November 08, 2004 with Dst = -374 nT. The minimum Dst intensity was approximate -374 nT at ~0700 UT, Nov 8, 2004.

Table 2 shows the Dst indices for each day considered in this work. The 6th day of November is considered a quiet day, and it will serve as a control for this study. Tables 3 to XX show the horizontal (DRMS) and the vertical (MRSE) errors and their average values for all the stations, concerning the various pseudorange measurements. The missing data (on Tables 6, 8 ..) were [A1][u2] because of unavailability of data owing to power outage in the various stations as at the time of real-time pseudorange measurement of positioning errors. These missing data is about 3% of the total data used and as such, can't have any significant effect the result. Vertical (MRSE) positioning errors were observed to be consistently greater than the horizontal (DRMS) positioning errors at low, mid and high latitude stations, for all pseudorange measurements. The difference between MRSE and DRMS shows the contribution of the vertical error. Table 23 shows a summary of the average values of positioning errors for different pseudorange measurements.

The L1 C/A and L1 P-code (single frequency) pseudorange measurement recorded lower average values of positioning errors compared to the average positioning errors from the L2 P-code single-frequency pseudorange measurement at all locations. The ionosphere affects L2 more than L1 since $f_1 = 1.57442$ GHz and $f_2 = 1.2276$ GHz. In the GPS L1 frequency where $f_{L1} = 1575.42$ MHz, one TECU corresponds to a delay of approximately 0.162 meters. Ionospheric delay is frequency dependent, i.e. under normal conditions, dual-frequency (L1 and L2) code and carrier observations can be used to remove ionospheric errors essentially.

The dual-frequency pseudorange measurement i.e. the Ionosphere-free combination (C/A on L1 and P on L2) and the ionosphere-free combination (P on L1 and P on L2) code largely recorded lower average values of positioning errors, and are far much better, reliable and accurate compared to the single-frequency pseudorange measurements, at low, mid and high latitude stations. A mid-latitude station (CRAO) recorded the highest average positioning horizontal and vertical errors of 50.563 m (L2 P-code) and 54.462 m (ionosphere-free combination C/A on L1 and P on L2 code) respectively as shown in Table 23 above. The lowest value for the average horizontal (1.83m) and vertical (3.86 m) errors is when Ionosphere-free L1/L2 combination (P on L1 and P on L2) measurement was used.

A careful comparison of errors from Tables 2-23, at low, mid and high latitudes show that geomagnetic storms and latitudinal variations do not have a very strong effect on positioning errors since relatively quiet days equally recorded high errors, i.e. the 6th and 12th days. Ionospheric scintillations due to plasma bubbles, multipath effect and other factors may have equally contributed to the errors.

Figures 2 – 4 show some of the east, the north and the up-positioning error (i.e. ENU) plots for selected stations at low, mid and high latitude stations, respectively. Figure 5 shows some of the GDOP, PDOP, and TDOP plots obtained for selected stations for a period. The GPS satellites are in constant

motion in different orbits. The figure shows changes in DOP values as a result of these movements. The TDOP and PDOP values are consistently smaller than the GDOP values. GDOP values are typically between 2 and 7. However, some stations do experience higher values above 8 and some spikes. A GDOP value greater than four depicts poor positioning of a GPS satellite during navigation, as compared to others.

DISCUSSION

During geomagnetic storms, plasma increase both in kinetic energy in the ionospheric medium. GPS signals passing through such medium become scattered, and as such suffers fluctuations in phase and amplitude due to small-scale irregularities. This effect is known as ionospheric scintillation, and it has a profound effect on GPS receivers, which subsequently leads to propagation delay (Aarons, 1982; Basuet *et al.*, 1988). GPS signals experience the most substantial propagation delay owing to severe space weather effects during the most geo-magnetically disturbed days, such as the 8th day [Day of the year (DOY): 313] of November 2004. Lower values of positioning errors along the Easting compared to the Up and Northing shows a lower horizontal error as compared to the 3-D vertical errors. Higher 3-D vertical errors than the horizontal errors indicate that GPS horizontal accuracies are far better compared to vertical accuracies since the variation of pressure, temperature and number density of gaseous molecules with altitude are more pronounced along vertical orientation than along horizontal direction (Rishbeth and Garriott, 1969). Another reason for the higher 3-D errors is because all the satellites from which the receivers obtain signals are above it. The horizontal position coordinates do not suffer a similar fate as they usually receive from all sides (Langley *et al.*, 1999).

Concerning the dual frequency ionosphere-free combinations, one would have expected a pretty low/zero positioning error value for the most magnetically quiet day (DOY: 311) if only the ionosphere is responsible for the positioning errors incurred by GPS radio signals traversing the atmosphere. The implication is that the possibility of other sources of errors apart from the ionosphere, like multipath, receiver noise, the effect of geometry (DOP) and ionospheric scintillation cannot be ruled out, and could have contributed to the values of positioning errors. Multipath errors occur when a signal reflects off nearby objects such as solid/semi-solid objects like mountains and buildings, before reaching the ground-based receiver. Receiver errors include noise generated in the receiver system and their varying ability to measure all signals equally. Better antennas and receivers can help minimise this error.

The dual frequency receivers provide more accurate and reliable pseudorange measurement owing to their ability to produce a first-order correction to the ionosphere. Pseudo-range measurements made with the ionosphere-free L1/L2 (dual frequency) combination (P on L1 and P on L2) relatively has low errors and hence more accurate positioning than measurements from the ionosphere-free L1/L2 (dual frequency) combination (C/A on L1 and P on L2). Pseudo-range measurements from the L1 P-code has relatively low errors and consequently, more accurate positioning compared to the L2 P-code measurements. Our result shows that dual-frequency GPS receivers are better than single-frequency receivers since dual-frequency GPS receivers can account for and remove error due to the ionosphere to some extent. Pseudo-range measurement

with the L2 P-code is the most inaccurate of all the measurements since it recorded larger values of positioning errors as compared to measurements on L1 C/A and L1 P codes. According to Misra and Enge (2006), a single frequency L1 C/A and L1 P codes pseudorange measurements are more reliable compared to a single-frequency L2 P-code pseudorange measurements. Adekunle (2004) affirmed that single frequency GNSS receivers are more vulnerable due to variations in the ionosphere, particularly at stations closer to the magnetic equator where large ionospheric variations occur.

The contribution to the positioning errors, inaccuracy and unreliability of the GPS from other sources like multipath, noise from the system cannot be ruled out since errors were recorded on quiet (i.e. low magnetically disturbed days). The Dilution of Precision (DOP) is commonly used to indicate the quality of satellite arrangement, and it is defined as the ratio of positioning accuracy to the observation accuracy (Langley *et al.*, 1999). It is one of the sources of positioning errors owing to poor positioning angles between satellites. The existence of wider angles between satellites observed for the various stations will ensure relatively low GDOP values, low positioning errors and higher reliability in GPS applications. DOP describes different satellite geometries, i.e. the location of the satellites in view relative to each other and the receiver. GDOP, PDOP and TDOP (time DOP) are the components of DOP. The poor GDOP recorded by nearly all the satellites indicate that satellites being used are not scattered but clustered near each other, throughout the sky, from the receiver's vantage point. The lower the value of GDOP, the better the ratio of position error to range error computing will be. GDOP plays an essential role in calculating the receiver's position using pseudorange measurements. The larger the number of satellites, the better the value of GDOP will be. PDOP values range from 1 to infinity; 1 - 4 results in correct positions, while 6 and higher indices indicate poor position (Langley *et al.*, 1999). Our result shows that GDOP values are typically between 2 and 7, with some stations experiencing values higher than 8. This shows poor positioning at those periods because a GDOP value greater than four depicts poor positioning of a GPS satellite during navigation.

The results of Groves *et al.* (2000) show that during active scintillation and ionospheric conditions, GPS receivers may experience navigation outages ranging from 20- to 90-min duration. This kind of navigation outages may have great implications on land, sea and air safeties as a result of poor positioning capabilities, especially around the equatorial region, including Nigeria. The problem will be more severe in Nigeria and other African countries because of the absence of GPS augmentation systems. Thus, it is essential for the introduction of augmentation systems in order to mitigate the effects of the ionosphere on GPS. However, there are several actions that GNSS service providers can take to lessen the impact and implications of the ionosphere. Increasing the number of satellites in the constellation is chief among them. The more satellites a user has before the onset of scintillations, the more likely the user will retain performance during a scintillation event. Therefore, incorporating as many satellites as possible in the present GNSS constellation is an effective means of mitigation.

CONCLUSION

Performance of space and ground-based navigation and communication GPS using different codes and carrier measurements, i.e. L1 C/A code, L1 P-code, L2 P-code and ionosphere-free combination (C/A on L1 and P on L2; P on L1 and P on L2), has been evaluated in this study. Data used for this research were from twenty ground-based GPS stations, from the 6th - 12th day of November 2004.

A summary of the main results obtained at low, mid and high latitudes stations are as follows:

- (a) Horizontal errors, i.e. DRMS, are far lesser compared to the 3-D vertical errors, i.e. MRSE. This implies that navigation systems record significant positioning errors vertically than horizontally.
- (b) The L2 P codes pseudorange measurement generally recorded larger values of positioning errors compared to the L1 C/A and the L1 P-code pseudorange measurement. Hence, single-frequency GPS receivers on L1 C/A and L1 P codes measurement are more accurate and reliable than the one on L2 P-code. Measurement on the ionosphere-free combination dual frequency receivers (C/A on L1 and P on L2) recorded more significant errors compared to the ionosphere-free L1/L2 combination (P on L1 and P on L2), but not as consistently high as the errors on the L2 P codes pseudorange measurement. Single frequency GNSS receivers are more vulnerable than dual frequency GNSS receivers to positioning error due to variations in the ionosphere. Hence, dual-frequency GPS receivers are better than single-frequency receivers
- (c) Our results show that geomagnetic storms are not strongly responsible for positioning errors, indicating that other factors like DOP, multipath and so on could also have accounted for these errors.
- (d) Positioning errors are not strongly dependent on latitudinal variation.

ACKNOWLEDGEMENT

The authors of this paper wish to sincerely thank International GPS Service (IGS) and Scripps Orbit and Permanent Array Centre (SOPAC) (<http://sopac.ucsd.edu>) for providing the GPS data for all stations. We equally appreciate Kugi-Kyoto (<http://wdc.kugi.kyoto-u.ac.jp/dstdir/index.html>) for providing the disturbed storm times Dst indices used for this research.

REFERENCES

- Aarons, J. (1982). Global morphology of ionospheric scintillations, *Proceedings of the IEEE* **70**, 360-378.
- Aaron, J. and Basu, S. (1994). Ionospheric amplitude and phase fluctuations at the GPS frequencies. *Proceedings of ION GPS* **94**, 1569-1578.
- Adekunle, I.O. (2014). An assessment of ionospheric error mitigation techniques for GNSS estimation in the low equatorial

- African region. *Positioning* **5(1)**: 27-35. doi: [10.4236/pos.2014.51004](https://doi.org/10.4236/pos.2014.51004).
- Adewale, A.O. Oyeyemi, E.O. Adeloje, A.B. Adedokun, M.B. (2013). Ionospheric effects of geomagnetic storms at Hobart and comparisons with IRI model predictions. *Journal of Scientific Research and Development* **14**: 98 – 105
- Adewale, A.O., Oyeyemi, E.O., Adeloje, A.B., Mitchel, C.N., Rose, J.A.R. and Cilliers, P.J. (2012). A study of L-band scintillations and total electron content at an equatorial station, Lagos, Nigeria. *Radio Science* **47(2)**: RS2011, <https://doi.org/10.1029/2011RS004846>
- Akala, A. O., Doherty, P. H., Carrano, C. S., Valladares, C. E. and Groves, K. M. (2012). Impacts of ionospheric scintillations on GPS receivers intended for equatorial aviation applications. *Radio Science* **47 (4)** RS4007, doi.org/10.1029/2012RS004995
- Bagiya, M. S. . Joshi, H. P. Iyer, K. N. Aggarwal, M. Ravindran, S. and Pathan, B. M. (2009). TEC variations during low solar activity period (2005–2007) near the equatorial ionospheric anomaly crest region in India. *Annales Geophysicae* **27**: 1047–1057.
- Basu, S. Mackenzie, E. and Basu, S. (1988). Ionospheric constraints on VHF/UHF communications links during solar maximum and minimum periods. *Radio Science* **23**: 363.
- Bent, R. B. Llewellyn, S.K. Nesterezuk, G. and Schmid, P.E. (1976). The development of a highly successful worldwide empirical ionospheric model, in Effect of the Ionosphere on Space Systems and Communications, J. Goodman (Eds). Nat. Tec. Inf. Serv., Springfield, Va, USA.
- Bhattacharya, S. Dubey, S. Tiwari, R. Purohit, P.K. and Gwal, A.K. (2008). Effect of magnetic activity on ionospheric time delay at low latitude. *Journal of Astrophysics and Astronomy* **29**, 269.
- Bhattacharya, S. Purohit, P. K. and Gwal, A. K. (2009). Ionospheric time delay variations in the equatorial anomaly region during low solar activity using GPS. *Indian Journal of Radio and Space Physics* **38(5)**: 266-274.
- Bilitza, D. and Reinisch, B. W. (2008). International reference ionosphere 2007: Improvements and new parameters. *Advances in Space Research* **42**: 599-609.
- Dashora, N. Sharma, S. Dabas R.S. Alex, S. and Pandey, R. (2009). Large enhancements in low latitude total electron content during 15 May 2005 geomagnetic storm in Indian zone. *Annales Geophysicae* **27(5)**: 1803-1820.
- Doherty, P. Delay, S. Valladares, C. and Klobuchar, J. (2000). Ionospheric scintillation effects in the equatorial and auroral regions, In: Proceedings of ION GPS-2000, Salt Lake City, pp662.
- Dubey, S. Wahi, R. and Gwal, A.K. (2006). Ionospheric effects on GPS positioning. *Advances in Space Research* **38** (11): 2478–2484.
- El-naggar, A. M. (2011). Enhancing the accuracy of GPS point positioning by converting the single frequency data to dual frequency data. *Alexandria Engineering Journal* **50(3)**: 237-243 <https://doi.org/10.1016/j.aej.2011.03.003>
- Goswami, S. Paul, A. and Haldar, S. (2018). Study of Relative Performance of Different Navigational Satellite Constellations Under Adverse Ionospheric Conditions. *Space Weather* **16(6)**: 667-675
- Groves, K.M. Basu, S. Quinn, J.M., Pedersen, T.R., Falinski, K. (2000). A comparison of GPS performance in a scintillation environment at Ascension Island, in: Proceedings of the ION GPS 2000, September 2000, Salt Lake City, UT, 2000.
- Hofmann-Wellenhof, B., Lichtenegger, H. and Collins, J. (2001). Global positioning system: Theory and practice, 5th Ed., Springer, Berlin
- Jain, At. Sunita T. Sudhir J. and Gwal, A.K. (2010). TEC response during severe geomagnetic storms near the crest of equatorial ionization anomaly. *Indian Journal of Radio and Space Physics* **39(1)**:11-24
- Jakowski, N. Schlüter, S. and Sardon, E. (1999). Total electron content of the ionosphere during the geomagnetic storm on 10 January 1997. *Journal of Atmospheric and Solar-Terrestrial Physics* **61(3)**: 299-307.
- Kintner, P. M. and Ledvina, B. M. (2005). The ionosphere, radio navigation, and global navigation satellite systems. *Advances in Space Research* **35(5)**: 788-811.
- Klobuchar, J. A. (1987). Ionospheric time-delay algorithm for single-frequency GPS users. *IEEE Transactions on aerospace and electronic systems* **3**: 325-331.
- Langley, R.B. (1999). Dilution of precision. *GPS World*, **10**: 52-59.
- Liu, J. Zhao, B. and Liu, L. (2010). Time delay and duration of ionospheric total electron content responses to geomagnetic disturbances. *Annales Geophysicae* **28**: 795-805, <https://doi.org/10.5194/angeo-28-795-2010>
- Misra, P. and Enge, P. (2006). GPS measurements and error sources. In: *Global Positioning System: Signals, measurements, and performance*, G. Gao and F. Walter (eds), Ganga-Jamuna Press, U.S.A., pp. 185-194.
- Nava, B. P. Coisson, and Radicella, S. M. (2008). A new version of the NeQuick ionosphere electron density model. *Journal of Atmospheric and Solar-Terrestrial Physics* **70(15)**: 1856-1862.

- Park, M.H. and Gao, Y. (2008). Error performance analysis of MEMS-based inertial sensors with low-cost GPS receiver. *Sensors* **8**: 2240-2261.
- Prasad, N. and Sarma, A. D. (2004). Ionospheric time delay estimation using IDW grid model for GAGAN. *Journal of Indian Geophysical Union* **8(4)**: 319-327.
- Radicella, S. M. and Leitingner, R. (2001). The evolution of the DGR approach to model electron density profiles. *Advances in Space Research* **27(1)**: 35-40.
- Rishbeth, H. and Garriott, O.K. (1969). Introduction to Ionospheric Physics, Academic Press, New York, pp 98-108.
- Sahai, Y. Fagundes, P. R. De Jesus, R. De Abreu, A. J. Crowley, A. J. G. Kikuchi, T. Huang, C.-S. Pillat, V.G. Guarnieri, F. L. Abalde, J.R. and Bittencourt, J.A. (2011). Studies of ionospheric F-region response in the Latin American sector during the geomagnetic storm of 21–22 January 2005. *AnnalesGeophysicae*. **29(5)**: 919–929.
- Skone, S. K. Knudsen, and De Jong, M. (2001). Limitations in GPS Receiver Tracking Performance Under Ionospheric Scintillation Conditions. *Physics and Chemistry of the Earth, Part A: Solid Earth and Geodesy* **26(6–8)**: 613-621.
- Trajkovski, K. K. Sterle, O. and Stopar, B. (2010). Study of positioning with high sensitivity GPS sensors under adverse conditions. *Sensors* **10(9)**: 8332-8347.
- Tsurutani, B. Anthony, M. Byron, I. Mangalathayil, A. A. Jose H. A. Sobral, Walter, G. Fernando, G. Toshitaka, T. Akinori, S. Kiyohumi, Y. Bela, F. Timothy J. Fuller-Rowell, Janet Kozyra, John C. Foster, AntheaCoster, and Vytenis M. Vasyliunas (2004). Global dayside ionospheric uplift and enhancement associated with interplanetary electric fields. *Journal of Geophysical Research: Space Physics* **109**: A08302, doi:10.1029/2003JA010342.
- Vlasov, M. Kelley, M. C. and Kil, H. (2003). Analysis of ground-based and satellite observations of F-region behavior during the great magnetic storm of July, 2000. *Journal of Atmospheric and Solar-Terrestrial Physics* **65**: 1223–1234.
- Yermolaev, Yu I. Zelenyi, L. M. Kuznetsov, V. D. Chertok, I. M. Panasyuk, M. I. Myagkova, I. N. Zhitnik, I. A. Kuzin, S. V. Eselevich, V. G. Bogod, V. M. Arkhangelskaja, I. V. Arkhangelsky, A. I. Kotov, Yu D. (2008). Magnetic storm of November, 2004: Solar, interplanetary, and magnetospheric disturbances. *Journal of Atmospheric and Solar-Terrestrial Physics* **70**, 334– 341
- Zhao, B. Wan, W. and Liu, L. (2005). Responses of equatorial anomaly to the October-November 2003 superstorms. *AnnalesGeophysicae* **23(3)**: 693–706.

Table 1: Latitude and Longitude of the stations (H – High Latitude; L – Low Latitude; M – Mid Latitude) واحد

Station Id	City	Location	Geographic latitude (°N)	Geographic Longitude (°E)	Geomagnetic Latitude (°N)	Geomagnetic Longitude (°E)	Region
Bake	Baker Lake	Canada	64.3	263.9	72.6	35.2	H
Eil1	Fairbanks	USA	64.7	212.9	65.4	95.1	H
Mcm4	Ross Island	Antarctica	-77.8	116.7	86.9	140.9	H
Whit	Whitehorse	Canada	60.8	224.8	63.7	79.9	H
Yell	Yellowknife	Canada	62.5	245.5	68.6	57.9	H
Iisc	Banglore	India	13	77.6	4.5	151	L
Kour	Kourou	French Guyana	5.3	307.2	14.3	20.5	L
Mkea	Mauna Kea	USA	19.8	204.5	20.6	86.3	L
Ajac	Ajaccio	France	41.9	8.8	42.4	90.2	M
Bucu	Bucuresti	Romania	44.5	26.1	42.1	107.7	M
Casl	Casey	Antarctica	-66.3	110.5	56.5	177.6	M
Chat	Waitangi	New Zealand	-43.9	183.4	45.3	94.4	M
Crao	Siemeiz	Ukraine	44.4	33.9	40.8	115	M
Davl	Davis	Antarctica	-68.6	77.9	59.7	159.1	M
Ebre	Roquetes	Spain	40.8	0.5	42.7	81.6	M
Vill	Villafranca	Spain	40.4	356	43.1	77	M
Well	Wellington	New Zealand	-41.3	174.8	44.1	104.1	M
Wes2	Westford	USA	42.6	288.5	52.1	1.5	M
Wgtn	Wellington	New Zealand	-41.3	174.8	44.2	104	M
Yakt	Yaktusk	Russian Federation	62	129.7	52.8	162.7	M

Table 2: Average Dst indices for study days in November 2004 **Table 2: اذنان**

DAYS	Dst VALUES (nT)
6th	10
7th	-117
8th	-374
9th	-214
10th	-259
11th	-106
12th	-92

Table 3: Showing the different positioning errors for ajac stations ثلاثة

Day	D_{st} (nT)	L1 C/A code		L1 P Code		L2 P Code		Ionosphere-free L1/L2 combination (C/A on L1 and P on L2)		Ionosphere-free L1/L2 combination (P on L1 and P on L2)	
		DRMS	MRSE	DRMS	MRSE	DRMS	MRSE	DRMS	MRSE	DRMS	MRSE
6th	10										
7th	-117	2.094	5.222	2.146	5.207	2.545	7.208	2.097	4.024	2.164	4.161
8th	-374	3.749	5.348	4.038	5.46	4.231	5.78	3.35	5.928	4.053	6.145
9th	-214	2.783	5.475	2.605	5.125	2.966	6.641	2.989	5.409	2.559	4.716
10th	-259	3.286	5.712	3.376	5.764	4.748	8.242	2.044	3.885	2.122	4.014
11th	-106	2.476	4.799	2.266	4.517	2.448	5.224	2.996	5.43	2.474	4.818
12th	-92	3.177	5.794	2.985	5.365	3.351	6.799	3.396	5.848	2.827	4.735
Average		2.928	5.392	2.903	5.240	3.382	6.649	2.812	5.087	2.700	4.765

Table 4: Showing the different positioning errors for bake stations أربعة

Day	DSt	L1 C/A code		L1 P Code		L2 P Code		Ionosphere-free L1/L2 combination (C/A on L1 and P on L2)		Ionosphere-free L1/L2 combination (P on L1 and P on L2)	
		DRMS	MRSE	DRMS	MRSE	DRMS	MRSE	DRMS	MRSE	DRMS	MRSE
7th	-117	2.716	6.701	2.785	6.888	3.341	8.296	2.409	5.769	2.377	6.031
8th	-374	3.738	8.590	3.833	8.815	4.666	10.183	3.265	7.663	3.082	7.734
9th	-214	2.550	5.356	2.359	5.396	2.845	6.363	2.759	5.010	1.958	4.630
10th	-259	2.302	6.402	2.228	6.318	2.611	6.988	2.418	6.402	2.072	5.954
11th	-106	2.448	5.572	2.257	5.272	2.365	5.668	2.937	6.270	2.264	5.175
12th	-92	2.288	5.472	2.115	5.198	2.326	5.755	2.624	6.205	2.024	5.038
Average		2.674	6.349	2.596	6.315	3.026	7.209	2.735	6.22	2.296	5.76

Table 5: Showing the different positioning errors for bucu Station خمسة

Day	Dst (nT)	L1 C/A code		L1 P Code		L2 P Code		Ionosphere-free L1/L2 combination (C/A on L1 and P on L2)		Ionosphere-free L1/L2 combination (P on L1 and P on L2)	
		DRMS	MRSE	DRMS	MRSE	DRMS	MRSE	DRMS	MRSE	DRMS	MRSE
6th	10	2.207	4.631	2.252	4.633	2.631	6.225	2.156	3.967	1.971	3.324
7th	-117	2.353	5.164	2.310	5.130	2.797	7.043	2.287	4.163	1.875	3.455
8th	-374	2.521	4.420	2.556	4.270	2.829	4.849	2.449	5.143	2.286	4.295
9th	-214	2.275	5.250	2.140	5.064	2.427	6.596	2.595	4.850	1.982	3.861
10th	-259	2.452	4.900	2.512	5.015	3.051	6.317	2.163	4.189	2.059	4.050
11th	-106	2.467	4.688	2.304	4.419	2.486	5.188	2.860	5.189	2.234	4.095
12th	-92	2.356	5.397	2.278	5.252	2.650	6.677	2.473	4.849	1.974	3.904
Average		2.376	4.921	2.336	4.826	2.696	6.128	2.426	4.621	2.054	3.855

Table 6: Showing the different positioning errors for casl Station ^{ستة}

Day	D_{st} (nT)	L1 C/A code		L1 P Code		L2 P Code		Ionosphere-free L1/L2 combination (C/A on L1 and P on L2)		Ionosphere-free L1/L2 combination (P on L1 and P on L2)	
		DRMS	MRSE	DRMS	MRSE	DRMS	MRSE	DRMS	MRSE	DRMS	MRSE
7th	-117	2.281	5.807			2.617	8.715	2.168	4.879		
8th	-374	3.624	8.670			3.941	9.285	3.577	8.813		
10th	-259	2.766	5.705			3.290	7.116	2.333	5.033		
11th	-106	2.912	7.083			3.027	7.397	2.984	7.746		
12th	-92	2.440	5.489			2.706	6.327	2.390	5.949		
Average		2.805	6.551			3.116	7.768	2.69	6.484		

Table 7: Showing the different positioning errors for chat Stati ^{سبعة}

Day	D_{st} (nT)	L1 C/A code		L1 P Code		L2 P Code		Ionosphere-free L1/L2 combination (C/A on L1 and P on L2)		Ionosphere-free L1/L2 combination (P on L1 and P on L2)	
		DRMS	MRSE	DRMS	MRSE	DRMS	MRSE	DRMS	MRSE	DRMS	MRSE
6th	10	1.992	5.613	2.029	5.711	2.349	7.995	2.000	4.692	2.330	4.579
7th	-117	2.323	5.981	2.396	6.221	3.049	8.928	2.257	4.202	2.450	4.572
8th	-374	4.157	7.178	4.280	7.245	6.051	10.386	3.184	6.471	2.911	5.794
9th	-214	2.400	4.606	2.228	4.580	2.419	5.390	5.292	2.840	2.521	5.021
10th	-259	11.333	16.113	11.181	15.863	3.738	7.048	3.092	6.309	2.574	5.369
11th	-106	1.913	4.565	1.879	4.403	3.240	7.255	3.991	8.127	4.169	7.901
12th	-92	1.840	4.236	1.818	4.156	2.118	5.794	2.142	4.64	2.075	4.113
Average		3.708	6.898	3.687	6.883	3.281	7.542	3.137	5.326	2.719	5.336

Table 8: Showing the different positioning errors for crao Station ^{ثمانية}

Day	D_{st} (nT)	L1 C/A code		L1 P Code		L2 P Code		Ionosphere-free L1/L2 combination (C/A on L1 and P on L2)		Ionosphere-free L1/L2 combination (P on L1 and P on L2)	
		DRMS	MRSE	DRMS	MRSE	DRMS	MRSE	DRMS	MRSE	DRMS	MRSE
6th	10	50.397	54.058			50.803	53.770	49.817	54.844		
7th	-117	50.807	54.207			51.406	54.040	49.927	54.850		
8th	-374	50.681	54.789			50.931	54.495	50.337	55.474		
9th	-214	49.322	52.969			49.572	52.669	48.975	53.756		
10th	-259	49.763	53.475			50.096	53.279	49.293	54.035		
11th	-106	49.954	53.684			50.186	53.473	49.544	54.125		
12th	-92	50.166	53.730			50.563	53.642	49.595	54.148		
Average		50.156	53.845			50.563	53.624	49.461	54.462		

Table 9: Showing the different positioning errors for davl Station ^{تسعة}

Day	D_{st} (nT)	L1 C/A code		L1 P Code		L2 P Code		Ionosphere-free L1/L2 combination (C/A on L1 and P on L2)		Ionosphere-free L1/L2 combination (P on L1 and P on L2)	
		DRMS	MRSE	DRMS	MRSE	DRMS	MRSE	DRMS	MRSE	DRMS	MRSE

6 th	10			2.231	5.271	2.645	6.911			1.906	5.059
7 th	-117			1.979	4.429	2.377	6.098			1.731	4.772
10 th	-259			1.798	4.520	1.804	4.514			1.951	5.172
11 th	-106			1.814	4.505	2.111	4.813			1.812	5.339
12 th	-92			2.020	4.575	2.341	4.976			1.759	5.171
Average				1.968	4.66	2.256	5.462			1.832	5.103

Table 10: Showing the different positioning errors for ebre station عشرة

Day	D_{st} (nT)	L1 C/A code		L1 P Code		L2 P Code		Ionosphere-free L1/L2 combination (C/A on L1 and P on L2)		Ionosphere-free L1/L2 combination (P on L1 and P on L2)	
		DRMS	MRSE	DRMS	MRSE	DRMS	MRSE	DRMS	MRSE	DRMS	MRSE
6 th	10	2.411	4.997			2.764	6.203	2.269	4.064		
7 th	-117	2.041	5.045			2.434	6.527	1.909	3.932		
8 th	-374	3.943	6.411			4.137	6.756	3.867	6.717		
9 th	-214	2.885	5.909			3.245	7.329	2.712	4.960		
10 th	-259	3.308	5.707			4.774	8.438	1.743	3.289		
11 th	-106										
12 th	-92										
Average		2.918	5.614			3.471	7.051	2.500	4.592		

Table 11: Showing the different positioning errors for eil station حدی عشر

Day	D_{st} (nT)	L1 C/A code		L1 P Code		L2 P Code		Ionosphere-free L1/L2 combination (C/A on L1 and P on L2)		Ionosphere-free L1/L2 combination (P on L1 and P on L2)	
		DRMS	MRSE	DRMS	MRSE	DRMS	MRSE	DRMS	MRSE	DRMS	MRSE
7 th	-117	2.794	6.436	2.786	6.492	4.077	14.422	3.812	19.358	3.698	19.29
8 th	-374	3.021	6.717	3.247	9.114	6.089	17.711	7.765	25.338	7.569	24.283
10 th	-259	2.125	4.604	1.966	4.644	8.541	19.534	13.100	30.467	12.916	30.059
12 th	-92	1.978	3.885	1.798	3.812	2.803	8.543	4.133	12.154	3.787	11.924
Average		2.48	5.411	2.45	6.016	5.378	15.053	7.203	21.83	6.993	21.389

Table 12: Showing the different positioning errors for vill Station اثنا عشر

Day	D_{st} nT	L1 C/A code		L1 P Code		L2 P Code		Ionosphere-free L1/L2 combination (C/A on L1 and P on L2)		Ionosphere-free L1/L2 combination (P on L1 and P on L2)	
		DRMS	MRSE	DRMS	MRSE	DRMS	MRSE	DRMS	MRSE	DRMS	MRSE
6 th	10	2.291	4.895	2.193	4.502	2.595	6.182	2.363	4.434	1.792	3.217
7 th	-117	1.897	5.274	1.897	5.249	3.320	9.045	1.936	3.824	1.636	3.708
8 th	-374	4.173	6.835	4.452	7.169	14.108	20.635	3.665	6.631	4.266	7.268
9 th	-214	2.799	6.211	2.636	5.707	51.024	69.777	2.948	5.533	2.241	3.951
10 th	-259	3.149	5.936	3.245	5.920	18.902	55.377	1.767	3.297	1.713	3.303
11 th	-106	2.632	5.765	2.361	5.156	98.051	14.914	3.202	6.505	2.308	4.824
12 th	-92	3.038	5.806	2.872	5.247	61.987	90.228	3.159	6.072	2.450	4.492
Average		2.854	5.817	2.808	5.564	35.712	38.023	2.72	5.185	2.344	4.395

Table 13: Showing the different positioning errors for well Station عشر ثلثة

Day	D_{st} (nT)	L1 C/A code		L1 P Code		L2 P Code		Ionosphere-free L1/L2 combination (C/A on L1 and P on L2)		Ionosphere-free L1/L2 combination (P on L1 and P on L2)	
		DRMS	MRSE	DRMS	MRSE	DRMS	MRSE	DRMS	MRSE	DRMS	MRSE
6 th	10	2.084	5.659	1.984	5.647	2.395	8.106	2.609	5.239	4.108	2.045
7 th	-117	2.557	6.335	2.507	6.375	3.396	9.344	2.665	5.011	2.190	4.117
8 th	-374	5.530	8.278	5.443	8.170	8.012	12.024	3.177	6.218	2.625	5.083
9 th	-214	2.403	4.574	2.171	4.447	2.353	5.479	3.092	5.577	2.313	4.484
10 th	-259	3.285	5.922	10.286	11.539	10.616	12.288	14.716	16.01	20.969	21.857
11 th	-106	1.708	3.773	1.538	3.467	1.677	4.575	2.559	5.110	1.885	3.490
12 th	-92	1.878	4.208	1.762	4.065	1.997	5.585	2.602	5.179	1.944	3.831
Average		2.778	5.536	3.67	6.244	4.349	8.200	4.489	6.909	5.184	6.415

Table 14: Showing the different positioning errors for wes2 Station عشر أربعة

Day	D_{st} (nT)	L1 C/A code		L1 P Code		L2 P Code		Ionosphere-free L1/L2 combination (C/A on L1 and P on L2)		Ionosphere-free L1/L2 combination (P on L1 and P on L2)	
		DRMS	MRSE	DRMS	MRSE	DRMS	MRSE	DRMS	MRSE	DRMS	MRSE
6 th	10	14.949	30.081			15.05	30.672	14.961	29.786		
7 th	-117	11.441	21.648			11.923	23.044	11.420	23.566		
8 th	-374										
9 th	-214	15.080	32.284			15.114	32.984	15.207	31.721		
10 th	-259	17.052	30.508			16.927	31.045	17.421	30.218		
11 th	-106	15.464	28.397			15.666	29.097	15.291	27.781		
12 th	-92	15.14	25.534			14.986	25.222	15.514	26.566		
Average		14.854	28.075			14.944	28.677	14.969	28.273		

Table 15: Showing the different positioning errors for wgn station عشر خمسة

Day	D_{st} (nT)	L1 C/A code		L1 P Code		L2 P Code		Ionosphere-free L1/L2 combination (C/A on L1 and P on L2)		Ionosphere-free L1/L2 combination (P on L1 and P on L2)	
		DRMS	MRSE	DRMS	MRSE	DRMS	MRSE	DRMS	MRSE	DRMS	MRSE
6 th	10	1.824	5.422	1.851	5.579	2.223	8.067	1.990	3.824	2.066	4.018
7 th	-117	2.462	6.298	2.485	6.467	3.321	9.378	2.256	4.127	2.348	4.353
8 th	-374	7.768	13.329	7.357	12.465	7.913	11.994	3.020	5.608	2.604	5.055
9 th	-214	2.337	4.555	2.195	4.565	2.341	5.550	2.750	4.885	2.449	4.754
10 th	-259	3.471	5.946	4.141	6.321	4.686	7.530	3.268	5.866	2.740	5.095
11 th	-106	1.613	3.674	1.528	3.579	1.650	4.642	2.120	4.162	1.922	3.681
12 th	-92	1.802	4.129	1.774	4.178	2.004	5.655	2.131	4.199	1.99	3.950
Average		3.040	6.193	3.047	6.165	3.448	7.545	2.505	4.667	2.303	4.415

Table 16: Showing the different positioning errors for whit station سنة عشر

Day	D_{st} (nT)	L1 C/A code		L1 P Code		L2 P Code		Ionosphere-free L1/L2 combination (C/A on L1 and P on L2)		Ionosphere-free L1/L2 combination (P on L1 and P on L2)	
		DRMS	MRSE	DRMS	MRSE	DRMS	MRSE	DRMS	MRSE	DRMS	MRSE
6th	10	2.732	6.051	2.679	5.995	2.867	7.230	2.854	5.830	2.576	5.098
7th	-117	3.021	6.474	3.089	6.626	3.936	7.927	2.501	5.874	2.476	5.799
9th	-214	2.285	5.759	2.203	5.660	2.473	6.760	2.774	6.083	2.304	5.266
11th	-106	2.717	4.540	2.737	4.708	2.706	5.167	3.022	4.799	2.907	4.637
12th	-92	2.102	4.207	1.991	4.213	2.058	5.058	2.523	4.467	2.074	3.814
Average		2.571	5.406	2.54	5.44	2.808	6.428	2.735	5.411	2.467	4.923

Table 17: Showing the different positioning errors for iisc station سبعة عشر

	Dst (nT)	L1 C/A Code (m)		L1 P Code (m)		L2 P Code (m)		Ionosphere-free L1/L2 Combination (C/A on L1 and P on L2) (m)		Ionosphere-free L1/L2 Combination (P on L1 and P on L2) (m)	
		DRMS	MRSE	DRMS	MRSE	DRMS	MRSE	DRMS	MRSE	DRMS	MRSE
6th	10	2.050	9.451	2.070	9.485	3.011	14.749	2.141	4.829	1.756	4.008
7th	-117	1.947	8.809	1.963	8.616	2.763	13.969	2.447	5.746	1.924	3.879
8th	-374	2.136	7.874	2.115	7.676	2.909	12.014	2.526	5.760	1.937	3.972
9th	-214	2.557	11.978	2.601	11.946	3.757	19.014	2.522	5.448	2.074	4.136
10th	-259	2.206	7.870	2.215	7.886	3.125	11.949	2.614	5.683	2.080	4.506
11th	-106	2.579	10.250	2.621	10.116	3.578	16.199	2.542	5.721	2.169	3.880
12th	-92	1.771	9.242	1.758	9.064	2.316	14.274	2.433	5.733	1.967	4.091
Average		2.178	9.353	2.192	9.256	3.066	14.955	2.461	5.560	1.987	4.067

Table 18: Showing the different positioning errors for kour station ثمانية عشر

Day	Dst (nT)	L1 C/A Code (m)		L1 P Code (m)		L2 P Code (m)		Ionosphere-free L1/L2 Combination (C/A on L1 and P on L2) (m)		Ionosphere-free L1/L2 Combination (P on L1 and P on L2) (m)	
		DRMS	MRSE	DRMS	MRSE	DRMS	MRSE	DRMS	MRSE	DRMS	MRSE
6th	10	3.575	10.516	3.540	10.688	5.247	15.573	2.139	5.467	2.007	5.420
7th	-117	3.041	9.669	3.040	9.851	4.678	14.929	1.740	4.359	1.522	4.092
8th	-374	4.465	12.637	4.490	12.938	6.559	19.005	2.261	5.498	2.165	5.959
9th	-214	4.236	11.566	4.179	11.751	6.455	18.894	2.495	4.919	2.088	4.325
10th	-259	2.327	8.091	2.364	8.306	2.996	12.872	2.026	4.637	1.791	4.205
11th	-106	3.400	9.167	3.321	9.184	4.556	13.988	2.771	5.472	2.154	4.355
12th	-92	3.376	10.894	3.421	10.900	5.452	16.799	2.171	6.482	1.757	4.961

Average		3.489	10.363	3.479	10.517	5.135	16.009	2.229	5.262	1.926	4.760
---------	--	-------	--------	-------	--------	-------	--------	-------	-------	-------	-------

Table 19: Showing the different positioning errors for mkea station تسعة عشر

Day	Dst (nT)	L1 C/A Code (m)		L1 P Code (m)		L2 P Code (m)		Ionosphere-free L1/L2Combination (C/A on L1 and P on L2) (m)		Ionosphere-free L1/L2 Combination (P on L1 and P on L2) (m)	
		DRMS	MRSE	DRMS	MRSE	DRMS	MRSE	DRMS	MRSE	DRMS	MRSE
6 th	10										
7 th	-117	4.046	11.831	3.958	11.613	5.736	17.013	2.680	6.252	2.231	5.334
8 th	-374	6.712	14.678	6.575	14.547	10.530	23.598	4.260	11.693	4.283	11.394
9 th	-214	4.714	12.636	4.614	12.332	7.730	20.467	5.422	10.054	5.549	9.824
10 th	-259										
11 th	-106	3.754	8.638	3.704	8.373	5.400	12.377	2.329	5.245	1.995	4.246
12 th	-92	3.494	7.332	3.438	7.066	5.200	10.800	2.141	5.776	1.711	4.729
Average		4.544	11.023	4.458	10.786	6.919	16.851	3.366	7.804	3.154	7.105

Table 20: Showing the different positioning errors for mcm4 station عشرون

Day	Dst (nT)	L1 C/A Code (m)		L1 P Code (m)		L2 P Code (m)		Ionosphere-free L1/L2Combination (C/A on L1 and P on L2) (m)		Ionosphere-free L1/L2 Combination (P on L1 and P on L2) (m)	
		DRMS	MRSE	DRMS	MRSE	DRMS	MRSE	DRMS	MRSE	DRMS	MRSE
6 th	10	2.050	9.451	2.070	9.485	3.011	14.749	2.141	4.829	1.756	4.008
7 th	-117	1.947	8.809	1.963	8.616	2.763	13.969	2.447	5.746	1.924	3.879
8 th	-374	2.136	7.874	2.115	7.676	2.909	12.014	2.526	5.760	1.937	3.972
9 th	-214	2.557	11.978	2.601	11.946	3.757	19.014	2.522	5.448	2.074	4.136
10 th	-259	2.206	7.870	2.215	7.886	3.125	11.949	2.614	5.683	2.080	4.506
11 th	-106	2.579	10.250	2.621	10.116	3.578	16.199	2.542	5.721	2.169	3.880
12 th	-92	1.771	9.242	1.758	9.064	2.316	14.274	2.433	5.733	1.967	4.091
Average		2.178	9.353	2.192	9.256	3.066	14.955	2.461	5.560	1.987	4.067

Table 21: Showing the different positioning errors for yakt station واحد و عشرون

Day	Dst (nT)	L1 C/A code		L1 P Code		L2 P Code		Ionosphere-free L1/L2 combination (C/A on L1 and P on L2)		Ionosphere-free L1/L2 combination (P on L1 and P on L2)	
		DRMS	MRSE	DRMS	MRSE	DRMS	MRSE	DRMS	MRSE	DRMS	MRSE
6 th	10			1.986	5.561	2.333	6.893			2.137	4.849
7 th	-117			2.871	5.665	3.421	7.229			2.667	4.923
8 th	-374			2.689	5.971	3.693	8.135			2.387	4.769
9 th	-214			2.233	5.121	2.768	6.512			2.273	4.900

10 th	-259			2.457	5.008	2.750	5.609			2.592	5.332
11 th	-106			2.030	4.953	2.097	4.823			2.455	5.212
12 th	-92			2.029	4.321	2.231	4.992			2.302	4.593
Average				2.328	5.229	2.756	6.313			2.402	4.94

Table 22: Showing the different positioning errors for yell station عشرون و اثنان نان

Day	D_{st} (nT)	L1 C/A code		L1 P Code		L2 P Code		Ionosphere-free L1/L2 combination (C/A on L1 and P on L2)		Ionosphere-free L1/L2 combination (P on L1 and P on L2)	
		DRMS	MRSE	DRMS	MRSE	DRMS	MRSE	DRMS	MRSE	DRMS	MRSE
6 th	10	2.165	5.879	2.159	5.827	2.300	7.097	2.530	5.423	2.220	4.833
7 th	-117	3.079	6.634	3.183	6.912	4.170	8.386	2.489	5.743	2.331	5.891
8 th	-374	3.283	8.500	3.378	8.665	4.120	9.938	2.979	7.682	2.835	7.679
Average		2.842	7.004	2.907	7.135	3.53	8.474	2.666	6.283	2.462	6.134

Table 23: Showing a summary of the average values of positioning errors for different pseudorange measurement ثلاثة و عشرون

Station Code	L1 C/A code		L1 P Code		L2 P Code		Ionosphere-free L1/L2 combination (C/A on L1 and P on L2)		Ionosphere-free L1/L2 combination (P on L1 and P on L2)	
	DRMS	MRSE	DRMS	MRSE	DRMS	MRSE	DRMS	MRSE	DRMS	MRSE
BAKE	2.674	6.349	2.596	6.315	3.026	7.209	2.735	6.22	2.296	5.76
EIL1	2.48	5.411	2.45	6.016	5.378	15.053	7.203	21.83	6.993	21.389
MCM4	2.178	9.353	2.192	9.256	3.066	14.955	2.461	5.56	1.987	4.067
WHIT	2.571	5.406	2.54	5.44	2.808	6.428	2.735	5.411	2.467	4.923
YELL	2.842	7.004	2.907	7.135	3.53	8.474	2.666	6.283	2.462	6.134
IISC	2.178	9.353	2.192	9.256	3.066	14.955	2.461	5.56	1.987	4.067
KOUR	3.489	10.363	3.479	10.517	5.135	16.009	2.229	5.262	1.926	4.76
MKEA	4.544	11.023	4.458	10.786	6.919	16.851	3.366	7.804	3.154	7.105
AJAC	2.928	5.392	2.903	5.24	3.382	6.649	2.812	5.087	2.7	4.765
BUCU	2.376	4.921	2.336	4.826	2.696	6.128	2.426	4.621	2.054	3.855
CHAT	3.708	6.898	3.687	6.883	3.281	7.542	3.137	5.326	2.719	5.336
CRAO	50.156	53.845			50.563	53.624	49.461	54.462		
EBRE	2.918	5.614			3.471	7.051	2.5	4.592		
VILL	2.854	5.817	2.808	5.564	35.712	38.023	2.72	5.185	2.344	4.395
WELL	2.778	5.536	3.67	6.244	4.349	8.2	4.489	6.909	5.184	6.415
WES2	14.854	28.075			14.944	28.677	14.969	28.273		
WGTN	3.04	6.193	3.047	6.165	3.448	7.545	2.505	4.667	2.303	4.415
CASL	2.805	6.551			3.116	7.768	2.69	6.484		
DAVL			1.968	4.66	2.256	5.462			1.832	5.103
YAKT			2.328	5.229	2.756	6.313			2.402	4.94

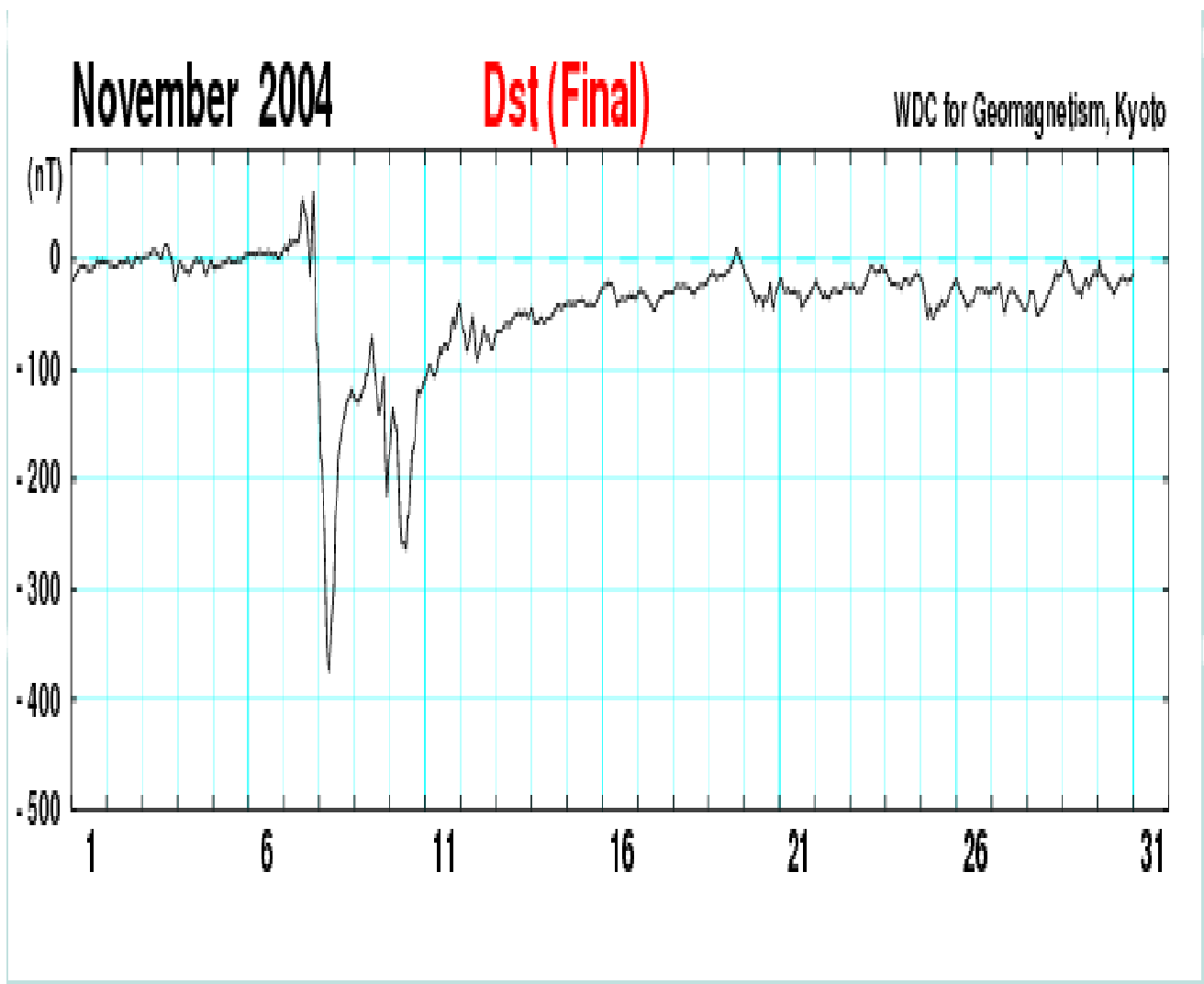


Figure 1: Dst values for November 2004 (from WDC for Geomagnetism, Kyoto)

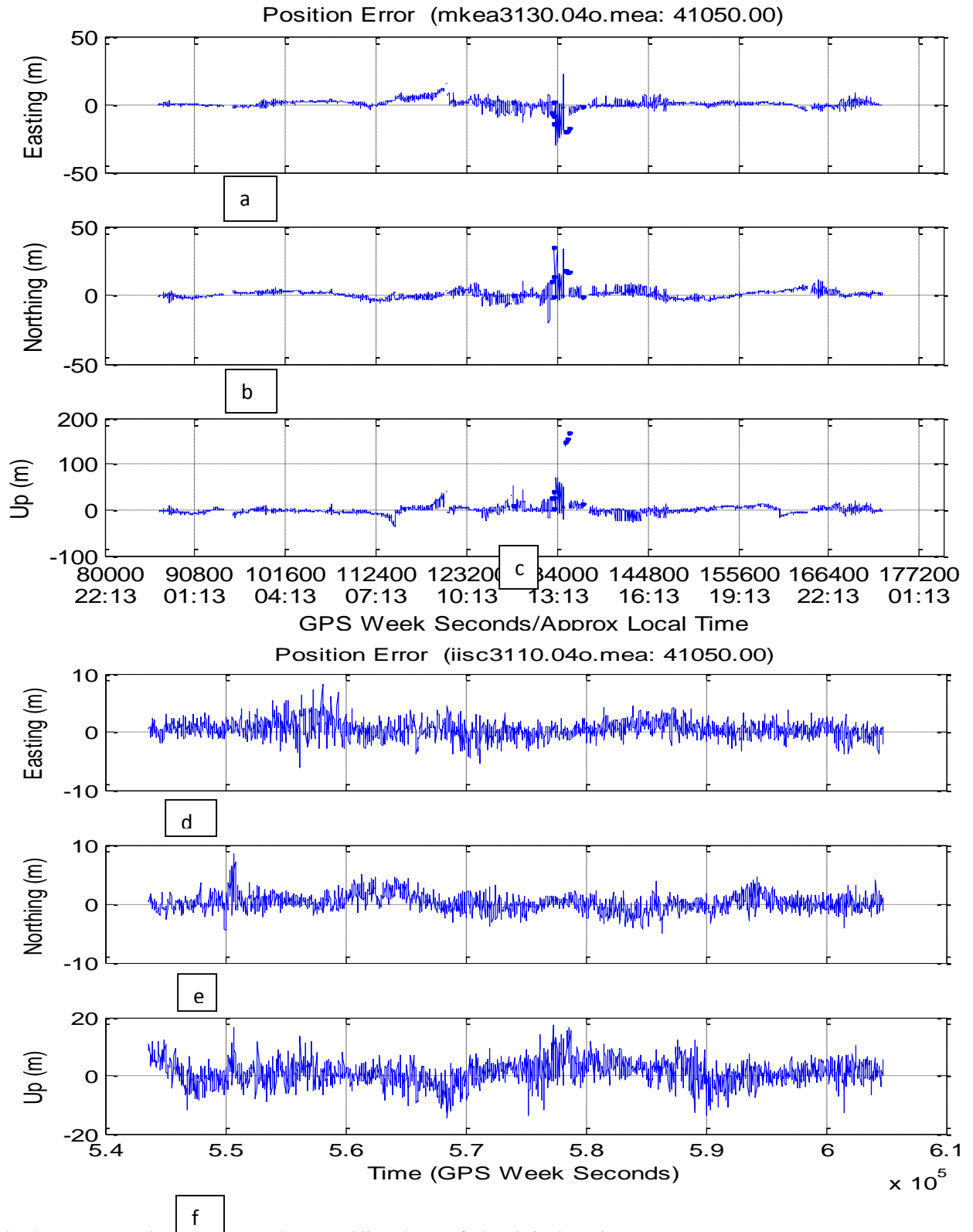


Fig. 2: The ENU error plot for mkea (a), (b), (c) and iisc (d), (e), (f) (low latitude stations)

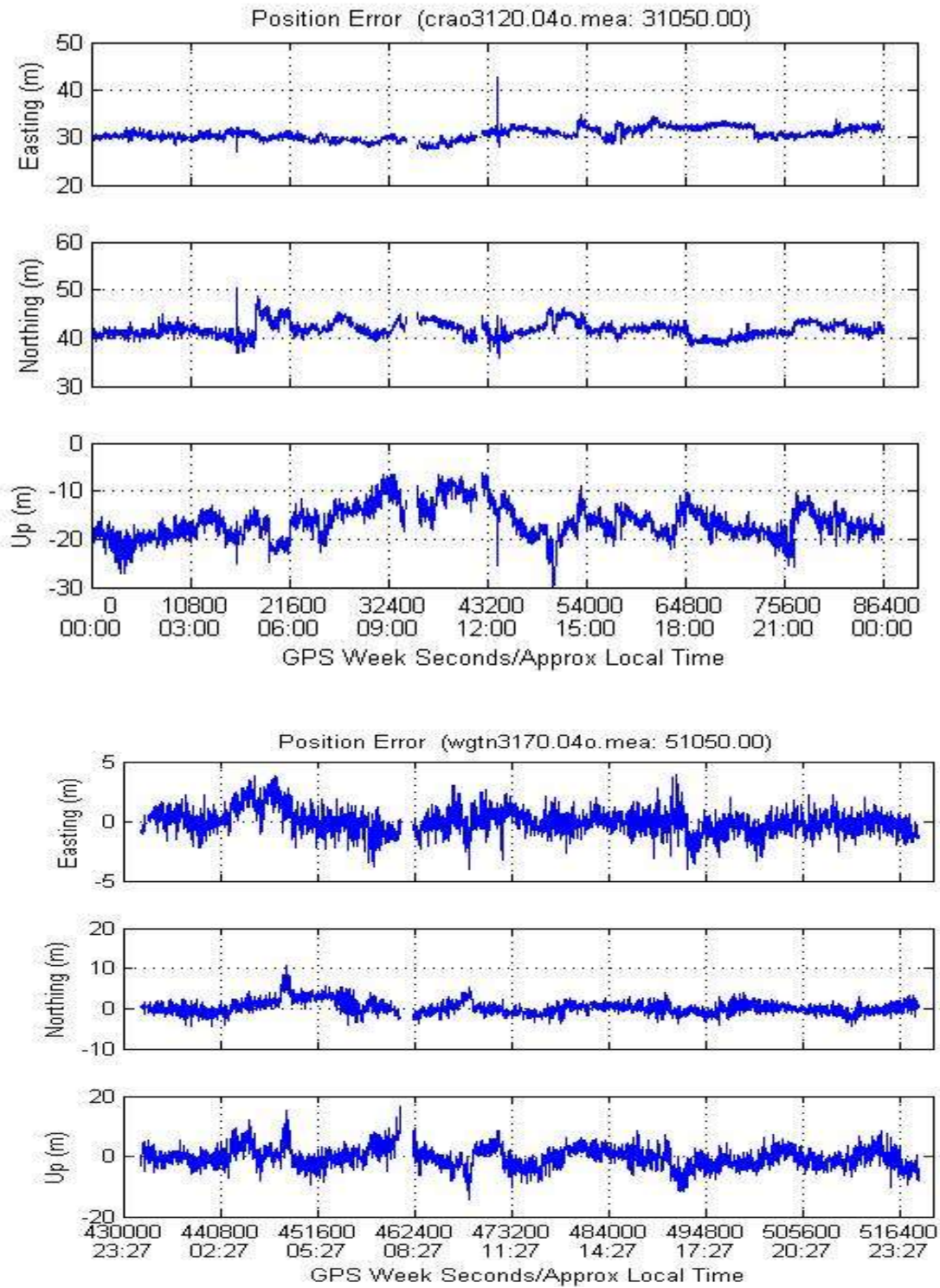


Fig. 3: The ENU error plot for crao3120.04o and wgn3170.04so (mid-latitude stations)

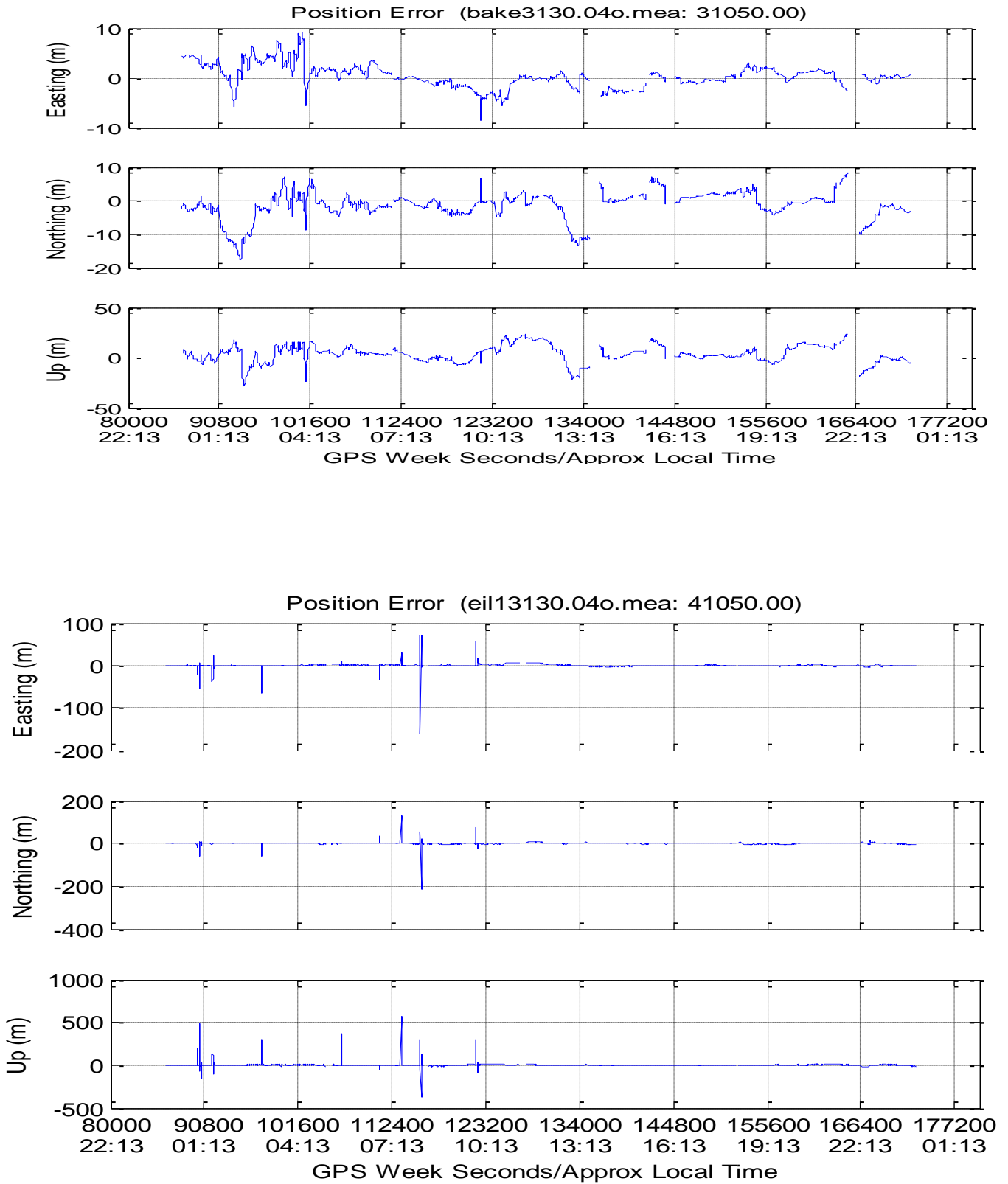


Fig. 4: The ENU error plot for bake and eil1 (high latitude stations)

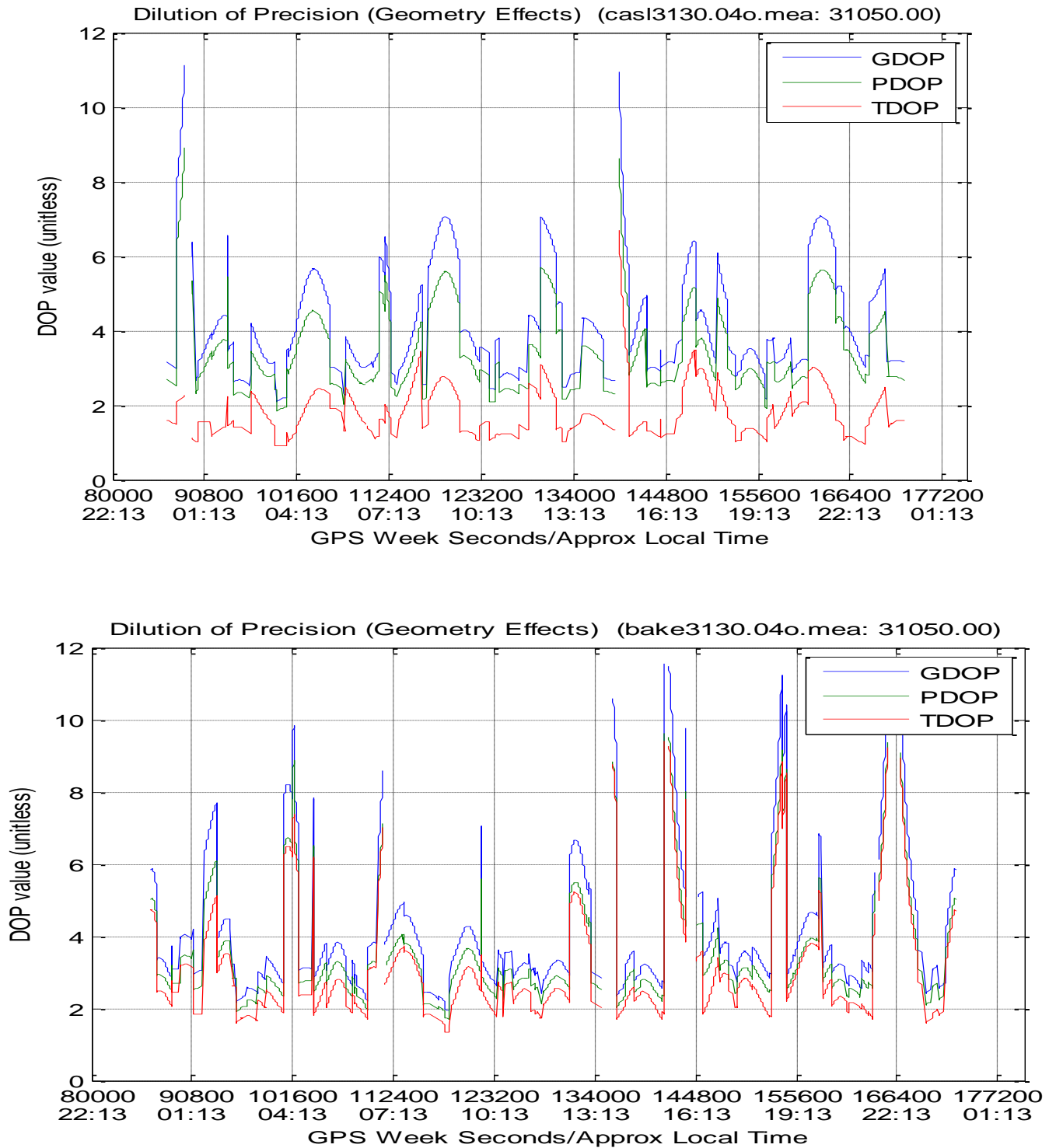


Fig. 5: Showing the GDOP, PDOP and TDOP plots for selected stations